Formation of multiple subpulses in a free-electron laser operating in the limit-cycle mode

G. M. H. Knippels,* A. F. G. van der Meer, R. F. X. A. M. Mols, D. Oepts, and P. W. van Amersfoort
Fundamenteel Onderzoek der Materie-Institute for Plasma Physics "Rijnhuizen," P.O. Box 1207, NL-3430 BE Nieuwegein, The Netherlands
(Received 10 July 1995)

The evolution of the longitudinal pulse shape and the spectrum of the short-pulse, far-infrared free-electron laser FELIX are investigated. Depending on the amount of cavity desynchronization applied, the laser is found to operate in the stable-focus mode or in the limit-cycle mode. In the latter case, autocorrelation measurements that are made with a setup that is based on second-harmonic generation in CdTe show the formation of a train of up to four subpulses. These are separated by the synchrotron length, and the corresponding sidebands in the spectrum are separated by the synchrotron frequency, in excellent agreement with theory. The measurements are made at a wavelength of 24.5 μm.

PACS number(s): 41.60.Cr

I. INTRODUCTION

In recent years, there has been a strong interest in the production of short, intense optical pulses in the far-infrared spectral range. This interest is driven mainly by the importance of these pulses for studies of the dynamic properties of a wide variety of semiconductor systems. Impressive progress has been made in the generation of intense pulses using nonlinear optical techniques, such as parametric oscillators [1–3]. However, there is a growing awareness that the free-electron laser (FEL) could well become the key player in this field. This is related to the fact that the FEL does not suffer from the transparency problems which are inevitably connected with the use of nonlinear crystals. The latter limits the spectral range in which intense pulses can be produced to wavelengths typically below 20 μm.

The absence of the transparency problem in an FEL is a consequence of the fact that laser radiation is generated and amplified in vacuum, by relativistic electrons traveling through the spatially periodic field of a so-called undulator magnet [4]. The radiation, which is emitted due to the periodic deflection of the electrons, is captured in an optical cavity and is amplified to saturation on successive passes through the undulator. An important feature of the FEL is the property of rapid and continuous tunability over a wide spectral range, which is achieved by adjustment of the electron energy and/or the undulator field strength [5].

The temporal structure of the laser output is related to the temporal structure of the driving electron beam. The latter consists of short bunches (with a duration of a few picoseconds) when a radio-frequency accelerator is used to accelerate the electrons. These bunches are separated by periods of zero current, which are a multiple of the period of the rf field. Consequently, also the laser beam consists of a train of short pulses.

The so-called slippage distance is a key parameter in the design and operation of a short-pulse FEL. This parameter gives the distance over which an electron bunch slips back relative to a stored optical pulse on their transit through the undulator, due to the fact that (i) the velocity of the electrons is somewhat smaller than the velocity of light and (ii) they move along an undulating path. The slippage distance is given by the product of the laser wavelength and the number of undulator periods [4]. It has often been anticipated that laser start-up would be "lethargic" in the case that the slippage distance is longer than the electron bunch length, i.e., that the gain per pass would be too small to achieve a saturated laser output. For this reason, most FEL's have been designed to operate in the regime of weak slippage, in which the slippage distance is (much) smaller than the bunch length. This includes the majority of rf-accelerator based FEL's, which use picosecond electron bunches but operate at wavelengths below 10 μm. The situation is different in rf-accelerator based FEL's for longer wavelengths. As an example, the free-electron laser for infrared experiments (FELIX) [6] covers the spectral range from 5 to 110 μm and uses electron bunches with a duration of the order of 3–6 ps [7]. In particular at the long-wavelength end of the spectral range, the slippage distance is thus (much) longer than the electron bunch length. The situation is similar for the long-wavelength FEL at Stanford [8] and possibly also for CLIO at Orsay [9].

The success of operation in the strong slippage regime is related to the fact that it has been realized that the "lethargy" phenomenon can be looked upon as a reduction of the optical group velocity [10]. The corresponding loss of synchronism of circulating optical pulses and electron bunches can be restored straightforwardly by a (slight) reduction of the length of the optical cavity, i.e., by a reduction of the round-trip time of the stored pulses. Depending on the amount of cavity length reduction (which is usually called "desynchronization") applied, either the gain per pass or the saturated power can be maximized [11].

*Author to whom correspondence should be addressed. Fax: +31-30-6031204. Electronic address: knippels@rijnh.nl

In spite of the usefulness of cavity desynchronization for circumventing a lethargic start-up, there is the problem that with a fixed cavity length it is impossible to maintain synchronism during the growth phase and during the saturated phase. This is due to the fact that the optical group velocity returns to the vacuum value as the stored power saturates. The corresponding loss of synchronism has the consequence that a new pulse can develop from the tail of the initial pulse. It has been predicted that eventually this leads to the formation of a train of subpulses, which are separated by a distance of the order of the slippage distance [12]. The underlying mechanism will be discussed in Sec. II. Needless to say, the formation of subpulses is undesirable for many applications, in particular for those that depend critically on a short pulse length.

The periodic growth and decay of subpulses leads to a modulation of the (time-averaged) power envelope. This limit-cycle oscillation has indeed been observed [12], but first attempts to visualize the subpulses by means of optical autocorrelation measurements were not very successful [11]. In this paper we report autocorrelation measurements made with a greatly improved setup, based on second-harmonic generation in CdTe [13]. The autocorrelator setup will be discussed in Sec. III.

A series of measurements of the evolution of the initially "clean" laser pulse into a train of subpulses will be presented in Sec. IV. The objective of the paper is twofold: (i) to confirm that the limit-cycle oscillation reported earlier in [12] is due to the formation of subpulses and (ii) to compare the experimental results with existing theoretical treatments. The latter is done in Sec. V and will provide the basis for our final objective: the production of clean pulses over the largest possible spectral range. Techniques for achieving this goal are under investigation already. Examples are dynamic desynchronization of the laser cavity [14] and the use of a step-tapered undulator field [15].

II. THEORETICAL BACKGROUND

Pulses FEL's can be characterized by the value of the longitudinal coupling parameter μ_c, which is defined as the ratio of the slippage distance $L_s = N\lambda$ (where N is the number of undulator periods and λ is the radiation wavelength) to the variance associated with the longitudinal electron density profile, σ_z [4]. In FEL's operating with values of μ_c that are smaller than unity, it has been observed that at saturation the initially smooth laser pulse breaks up into a train of short spikes [16], separated by the slippage distance [17]. This is related to the fact that, at a high stored field, the electrons are bunched efficiently at the early stages of the undulator (and therefore emit intense radiation) but can reabsorb part of the radiation at the later stages, due to the oscillation of the electron bunch in the ponderomotive potential which is formed by the combined undulator and laser fields. In combination with slippage, this reabsorption leads to a longitudinal modulation of the optical field intensity.

In FEL's operating with a value of μ_c greater than unity, i.e., with electron bunches shorter than the slippage distance, Hahn and Lee showed theoretically that the spikes are not separated by the slippage distance but by the so-called synchrotron length [17]. The synchrotron length is the slippage experienced by the electrons during a synchrotron oscillation period in the ponderomotive potential. Therefore, FEL operation (at $\mu_c > 1$) with electron bunches shorter than the synchrotron length characterizes a regime which is distinctly different from the spiking mode: since each spike extracts energy from the electron bunch over a length that is equal to half the synchrotron length, an electron bunch shorter than L_{syn} implies that only a single spike can grow *within the electron bunch.* However, at saturation this optical pulse moves forward on successive round trips due to the applied cavity desynchronization and therefore loses contact with the electrons. The pulse subsequently decays because there is round-trip loss, while a new pulse is generated by the electron bunch, at a distance of one synchrotron length behind the first pulse [17]. The process is then repeated with this new pulse. The formation of a train of subpulses leads to a stable limit-cycle oscillation of the macropulse power, which is quite different from the irregular modulation observed in spiking FEL's [18]. The limit-cycle regime is considered in this paper.

Hahn and Lee have found that the various regimes of FEL operation can be identified with the parameter $\mu = L_s / L_{\text{syn}}$ [17]. The radiation pulse remains quasicontinuous in the stable-focus region ($\mu < 0.8$), i.e., no subpulses develop. The range $0.8 < \mu < 1.5$ is identified as the limit-cycle region. The sidebands in the spectrum, which are present due to the existence of subpulses, double sequentially in the period-doubling region, $1.5 < \mu < 2.0$. Finally, the chaotic regime is characterized by $\mu > 2$. To reach the regime where $\mu > 1$, L_{syn} has to become smaller than L_s. This means that the intracavity power has to saturate at a sufficiently high level.

An *ab initio* calculation of the intracavity power (in order to determine the value of μ) is nontrivial and requires, for instance, knowledge of the electron bunch length. Note that the optical power saturates when the corresponding synchrotron length approaches the electron bunch length. However, for a working FEL one can estimate the intracavity power from the measured output power and the pulse duration. This gives an estimate of L_{syn}, which in our analysis is compared to the measured subpulse separation.

For the determination of the intracavity power, the dimensionless complex optical field, $a = |a| \exp(i\phi)$, is expressed as [19]

$$|a| = (4\pi N)^2 \frac{K}{1+K^2} [J_0(\xi) - J_1(\xi)] \frac{e\lambda E}{2\sqrt{2}\pi mc^2} \tag{1}$$

$$\xi = \frac{1}{2} \frac{K^2}{1+K^2} , \tag{2}$$

where K is the (rms) undulator strength and E is the envelope of the complex electric field. The parameter K is a dimensionless parameter proportional to the peak magnetic field, B_u, in the undulator,

$$K=\frac{eB_u\lambda_u}{2\sqrt{2}\pi mc},$$

where λ_u, e, m, and c are the length of an undulator period, the electron charge, the electron rest mass, and the vacuum velocity of light, respectively. The Bessel functions J_0 and J_1 account for the fact that a planar undulator is used. The synchrotron frequency Ω in the observer's frame is defined as [20,21]

$$\Omega=\frac{c}{N\lambda}\sqrt{|a|} \tag{3}$$

and the slippage of the electrons during the execution of a cycle of the synchrotron oscillation is [17]

$$L_{\text{syn}}=\frac{\lambda_u}{\lambda_u-\lambda}\frac{2\pi c}{\Omega}. \tag{4}$$

The value of L_{syn} can be calculated from Eqs. (1)–(4), if the electric field amplitude E is known. An estimate of the intracavity power allows us to calculate the intracavity electric field since

$$P=\tfrac{1}{2}c\varepsilon_0 AE^2, \tag{5}$$

where A is the mode area in the cavity at the waist position. This area is given by

$$A=\frac{\pi^2 L_u\lambda}{8} \tag{6}$$

under the assumption of a transverse Gaussian beam profile (with a radius enclosing 99% of the power [22]), and use of the fact that at FELIX the Rayleigh length equals half the undulator length L_u [5]. Combination of Eqs. (5) and (6) results in an electric field of

$$E=\left[\frac{16P}{c\varepsilon_0\pi^2 L_u\lambda}\right]^{1/2} \tag{7}$$

which enables the calculation of L_{syn} for a given value of the intracavity power. The latter can be estimated from the measured energy loss of the electrons and the measured cavity decay time. Using the measured optical pulse duration this can be converted to intracavity peak power, see Sec. V.

III. EXPERIMENTAL SETUP

In the experiment reported here, we use the short-wavelength FEL of the user facility FELIX [6], which covers the spectral range between 5 and 35 μm. The optical output consists of (sub)picosecond micropulses which are repeated at a frequency of 1 GHz. The micropulses form a train, the so-called macropulse, with a duration of typically 10 μs. The optical cavity has a length of 6.15 meter, which has the consequence that 41 optical pulses circulate in the cavity. Radiation is coupled out through a 2-mm-diam hole in one of the mirrors. The radiation is guided to the autocorrelator setup via an evacuated transport system. The average output power in a macropulse, measured at the autocorrelator, is typically 20 kW.

The second-order autocorrelator setup, which is based on second-harmonic generation (SHG) in CdTe [23], is shown in Fig. 1. Broad wavelength coverage with a single crystal is possible because of the large transparency range (1–35 μm) and low dispersion of CdTe. Since CdTe is not birefringent (the refractive index ranges from 2.7 to 2.5 between 5 and 35 μm), phase matching is impossible. However, the low dispersion makes it possible to generate a detectable amount of second-harmonic radiation in a single coherence length. The latter ranges from 190 μm at 10-μm radiation wavelength to 60 μm at 35-μm wavelength. In view of the destructive interference of the second-harmonic radiation emitted in subsequent coherence lengths, the thickness of the crystal must be an odd multiple of the coherence length. Therefore, the crystal is cut in a wedge (0.75–0.98 mm) in order to have the possibility to select the optimum thickness for each operating wavelength. Furthermore, the absence of a (critical) phase-matching angle makes the amount of generated second-harmonic radiation rather insensitive to the orientation of the crystal.

The well-known crossed-beam setup is used to produce a fringe-free, zero-background autocorrelation signal [24]. The angle between the crossed beams in the crystal is limited to 5°, in order to minimize overestimation of the pulse duration due to the finite transverse beam dimensions [25]. Furthermore, group-velocity mismatch is negligible over the whole wavelength range, but lengthening of the fundamental pulse in the crystal due to dispersion limits the temporal resolution to 150 fs at 10-μm wavelength and to 350 fs at 24 μm. Because of the low conversion efficiency (estimated between 10^{-4} and 10^{-6}), the use of blocking filters for higher harmonics that are present in the FELIX output is essential. These harmonics contain roughly 0.1–1 % of the total energy. A set of coated germanium filters (Barr Associates, Yattendon, UK) with a transmission of 50% at the fundamental and

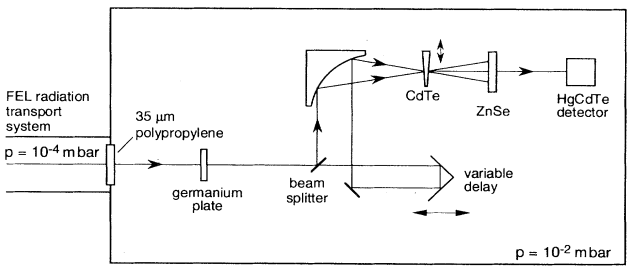

FIG. 1. Second-order autocorrelator setup, based on second-harmonic generation in a wedge-shaped single-crystalline sample of CdTe. A crossed-beam setup is used for obtaining a zero-background fringe-free signal. A mirror, which scrapes off part of the beam, is used as a beamsplitter. The second-harmonic radiation is measured with a HgCdTe detector (response time < 50 ns). The fundamental frequency is blocked in front of the detector by either ZnSe, CaF_2, or sapphire, depending on the operating wavelength. Harmonics in the FEL output are blocked by coated germanium filters. The whole setup is evacuated to avoid pulse distortion by absorption in ambient water vapor.

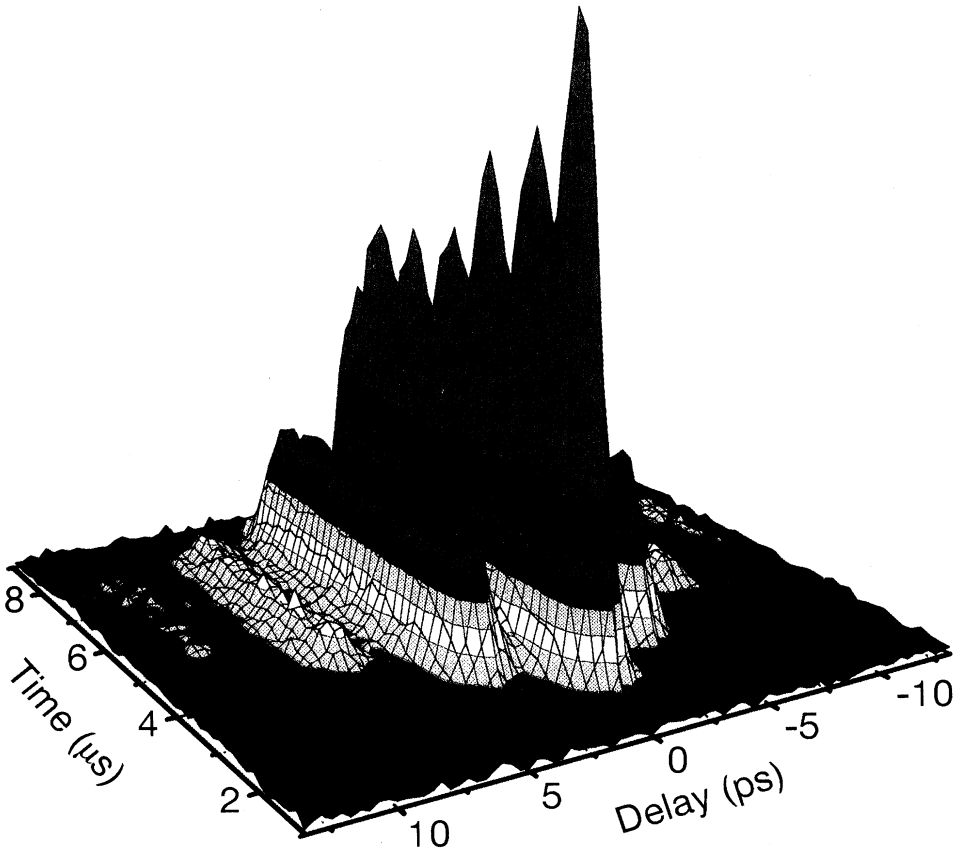

FIG. 2. Second-order autocorrelation signal versus time in the macropulse. The laser wavelength is 24.5 μm and the applied cavity desynchronization ΔL is -16 μm. The development into a train of four separate subpulses is observed (these four pulses show up as seven peaks in the autocorrelation signal). The colors serve for illustration purposes.

a transmission for harmonics of less than 0.1% give the necessary background reduction (in combination with the crossed-beam setup). Blocking of the fundamental frequency after SHG in the crystal is achieved by a plate of either ZnSe (5 mm), CaF_2 (2 mm), or sapphire (3 mm), depending on the operating wavelength.

An advantage of the crossed-beam setup is the fact that it allows the use of a mirror to scrape off part of the beam, instead of a (wavelength-dependent) dielectric beam splitter foil in a Michelson interferometer setup. This method of beam splitting alleviates the problems connected with dielectric beam splitters, namely limited transmission, pulse shape distortion due to dispersion, multiple reflections in the foil, and deviations from the desired 1:1 splitting ratio. Hence, when the FEL wavelength is changed, only the set of blocking filters has to be changed and the second-harmonic signal can be optimized by selecting the optimum thickness of the CdTe crystal. This is done by translating the crystal. Although the use of a mirror gives some diffraction of the beam, it is still possible to produce a good focus on the crystal.

A high signal-to-noise ratio in the second-harmonic signal is possible because of the high damage threshold of the CdTe crystal. This allows focusing of the full FEL output power on the crystal. Power densities of up to 25 GW/cm^2 have been applied without any visible damage to the crystal surface. A liquid-nitrogen cooled HgCdTe detector with a response time of less than 50 ns is used for detection of the second-harmonic radiation. The complete autocorrelator setup is evacuated to roughly 10^{-2} mbar in order to avoid distortion of the optical pulse due to absorption of the infrared radiation by ambient water vapor. The setup is connected to the evacuated FEL-radiation transport system by a 35-μm-thick polypropylene window, or by a ZnSe window when operating at a wavelength below 15-μm wavelength. The time needed to scan the variable delay sets the time to measure an autocorrelation trace to typically two minutes. Since the autocorrelation trace is taken over typically 200 macropulses, triggering on the leading edge of the macropulse is essential to removing the influence of shot to shot fluctuations in the laser start-up.

A spectrometer (SpectraPro VM-504, Acton Research, Massachusetts) with a 48-channel pyroelectric array is used to record the optical spectrum of each macropulse. Each channel is sampled at a frequency of 5 MHz (12 bits resolution) and the bandwidth is 600 kHz. The spectrometer is equipped with a turret containing three gratings to cover the wavelength range from 5 to 100 μm. A pyroelectric detector with a response time of 100 ns is used to record the optical macropulse. This pyroelectric detector and the optical spectrometer are also evacuated to eliminate absorption by water vapor.

IV. EXPERIMENTAL OBSERVATION OF SUBPULSES

An example of the evolution of the second-order autocorrelation signal is shown in Fig. 2, as measured at a FEL wavelength of 24.5 μm and a cavity desynchronization of $\Delta L = -16$ μm. The electron energy was 37.5

MeV. The delay axis corresponds to the change in optical path length introduced by scanning one arm of the autocorrelator, while the time axis corresponds to the time in the macropulse. The autocorrelation signal indicates a single pulse, around zero delay, during the early stages of the macropulse. This pulse splits up into (finally) four separate pulses; note that n pulses in the time domain appear as $2n-1$ peaks in the autocorrelation signal. In the remainder of this paper we will have a closer look at the autocorrelation signal at fixed times in the macropulse. No further averaging or smoothing of the measurements is performed, except when mentioned explicitly. However, we do necessarily average over roughly 50 consecutive micropulses, due to the 50-ns response time of the HgCdTe-detector and the 1-ns separation between the micropulses.

The evolution of the subpulses depends strongly on the applied cavity desynchronization. Therefore we measured three macropulses at 24.5-μm wavelength, shown in Figs. 3(a)–3(c), at different cavity desynchronizations of $\Delta L=-3$ μm, $\Delta L=-16$ μm, and $\Delta L=-50$ μm, respectively, and at an electron energy of 37.5 MeV. The electron macropulse is switched off at $t=7.0$ μs. Only in Fig. 3(b) a clear limit-cycle oscillation is observed. The absence of limit cycles in Fig. 3(a) is due to the fact that the electron macropulse cannot be sustained long enough to see them evolve. Note that the small value for ΔL in Fig. 3(a) leads to a high saturated power level but to a low small-signal gain per pass, which gives rise to a long time needed to reach saturation. An increase of the cavity desynchronization, as in Fig. 3(b), improves the overlap between the electron bunches and the optical pulses during signal buildup and therefore saturation is reached earlier. A limit-cycle oscillation is observed in the saturated part of the optical macropulse. When an even larger cavity desynchronization is applied, as in Fig. 3(c), the oscillation disappears. This is related to the decrease of the optical power to a level where no reabsorption of the radiation field by the electrons takes place, i.e., the "stable-focus" regime [17]. This will be discussed further in Sec. V.

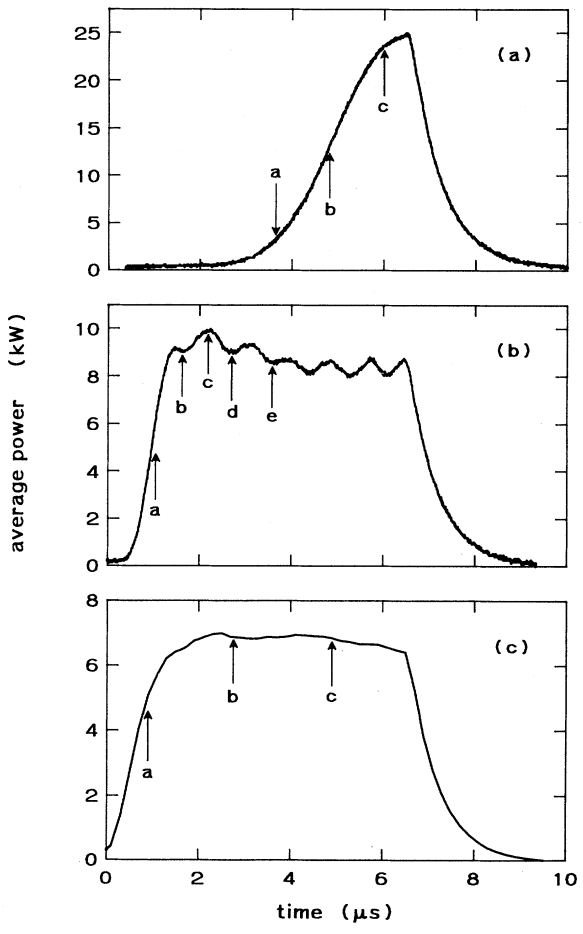

FIG. 3. Average FELIX output power versus time, for a wavelength of 24.5 μm. Cases (a), (b), and (c) correspond to cavity desynchronizations of, respectively, $\Delta L=-3$ μm, $\Delta L=-16$ μm, and $\Delta L=-50$ μm. The electron pulse is switched off at $t=7.0$ μs. The second-order autocorrelation traces and power spectra for the moments indicated by the arrows in (a), (b), and (c) are presented in, respectively, Figs. 4, 5, and 6.

In Figs. 3(a)–3(c) several instants in the three macropulses are indicated by arrows. The second-order autocorrelation signals (left-hand side) and the optical spectra (right-hand side) at these moments are plotted in Figs. 4–6. In Fig. 4 optical pulse shapes are observed without any trace of subpulses, for the macropulse of Fig. 3(a). The $\mathrm{sech}^2(t)$ fits to the autocorrelation measurements indicate an FWHM pulse duration of 610, 540, and 500 fs for Figs. 4(a)–4(c), respectively. The gradual shortening of the pulse as saturation is approached is a consequence of the reabsorption of field energy at the trailing edge of the pulse, under the combined influence of the synchrotron oscillation and slippage [26]. The FWHM of the power spectra in Figs. 4(a) and 4(b) are measured to be 5.6% and 7.9%, respectively, leading to a time-bandwidth product of 0.41 and 0.50. The time-bandwidth product for an ideal $\mathrm{sech}^2(t)$-shaped pulse is 0.31 [27]. It is interesting to note that the pulse in Fig. 4(c) contains only six cycles of the optical field at the FWHM, which is comparable to the number of cycles in the shortest pulses reported in the visible [28] and near-infrared spectral regions [29] for other types of lasers. The modulation in the spectrum in case (c) suggests some feature in the time domain around 5-ps delay. This is currently under investigation.

In Fig. 5 a similar series of measurements is shown for the instants indicated in the macropulse of Fig. 3(b). The initially smooth pulse in (a), with a FWHM pulse duration of 810 fs [as derived from a $\mathrm{sech}^2(t)$-fit] and smooth spectrum with a FWHM of 3.1%, evolves into two separate subpulses, i.e., three peaks in the autocorrelation signal (b). This situation corresponds to the moment when the minimum in the first limit-cycle period is reached, which is the moment that the initial pulse has lost contact with the electron bunch. A subpulse develops at its trailing edge, separated by 1.0-mm distance (corresponding to the measured 3.5-ps delay), and grows to saturation. In the optical spectrum this subpulse

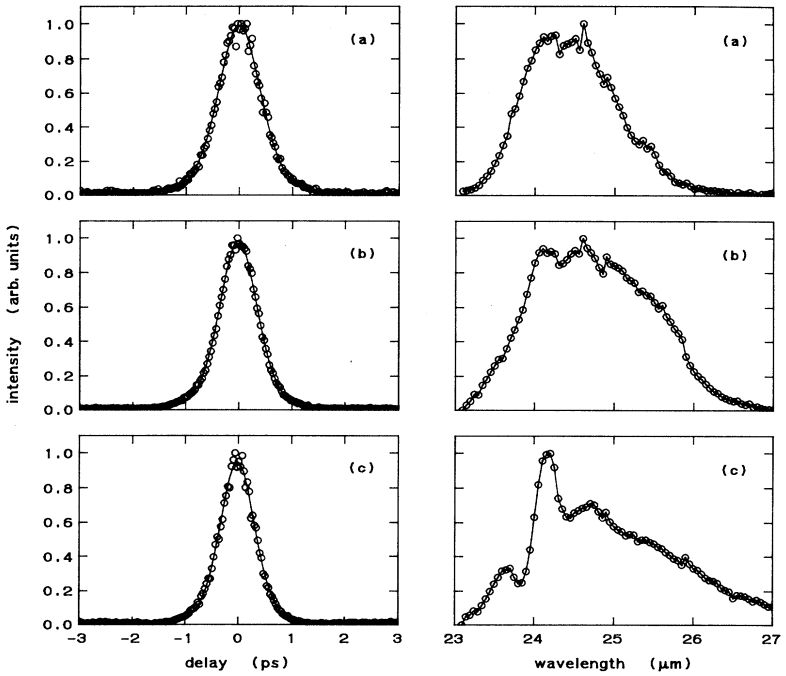

FIG. 4. Second-order autocorrelation traces (left-hand side) and optical power spectra (right-hand side), for three different instants (a)–(c) in the macropulse of Fig. 3(a), when a cavity desynchronization of $\Delta L = -3$ μm is applied. The solid lines in the autocorrelation measurements represent a $\mathrm{sech}^2(t)$ fit. The derived FWHM pulse durations in cases (a)–(c) are, respectively, 610, 540, and 500 fs, and the pulse energy in (c) is 25 μJ.

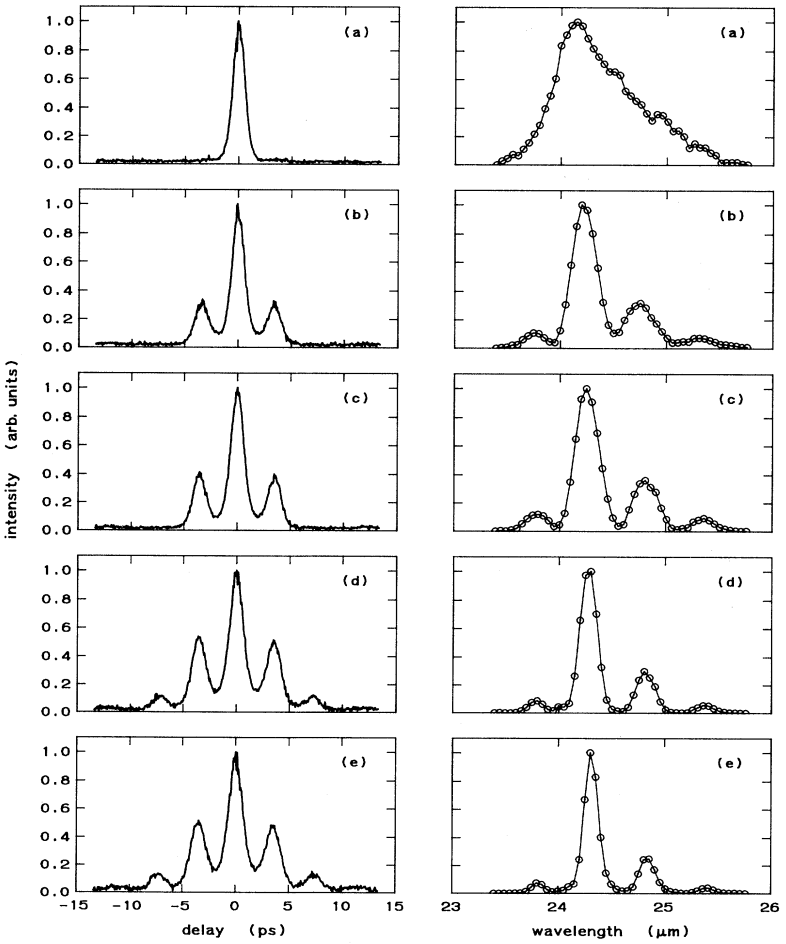

FIG. 5. Second-order autocorrelation traces (left-hand side) and optical power spectra (right-hand side), for five different instants (a)–(e) in the macropulse of Fig. 3(b), when a cavity desynchronization of $\Delta L = -16$ μm is applied. The FWHM pulse duration in (a), assuming a $\mathrm{sech}^2(t)$-shaped pulse, is 810 fs, and the energy is 8.0 μJ. The development of a train of four subpulses is observed in (b) to (e). The corresponding sidebands in the spectrum narrow upon formation of each new pulse.

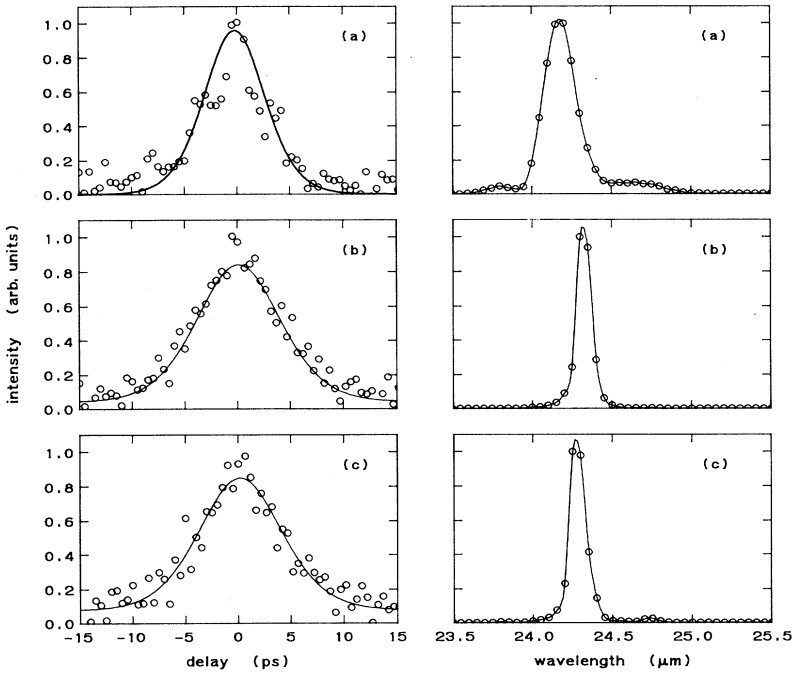

FIG. 6. Second-order autocorrelation traces (left-hand side) and optical power spectra (right-hand side), for three different instants (a)–(c) in the macropulse of Fig. 3(c), when a cavity desynchronization of $\Delta L = -50$ μm is applied. The solid lines in the autocorrelation measurements represent a $\mathrm{sech}^2(t)$ fit. The derived FWHM pulse durations in cases (a)–(c) are, respectively, 4.4, 6.0, and 6.0 ps. The pulse energies are 5.0 μJ in case (a) and 7.0 μJ in cases (b) and (c).

shows up as a series of sidebands. At the moment that the next maximum is reached in the limit-cycle period (c), a more or less identical autocorrelation trace is measured as in (b), but now the subpulse present at the trailing edge is about as large as the leading pulse, as can be seen from the ratio of 0.4 between the intensity of the main peak and the side peaks. A ratio of 0.5 is expected for two identical pulses.

The evolution is repeated in the next period of the limit cycle, as seen in Fig. 5(d), with the distinction that the remnants of the first pulse are still visible at a delay of 7.0 ps. This is possible due to the small cavity loss per round trip (5%). The growing train of subpulses with a fixed distance between them shows up in the optical spectrum as a narrowing of the series of sidebands, as expected from the Fourier theorem. Finally, in Fig. 5(e) the fourth pulse has formed, which still mixes with the low-intensity first pulse to produce a tiny signal at 11-ps delay.

A similar series of measurements with a cavity desynchronization of $\Delta L = -50$ μm is shown in Fig. 6. The autocorrelation signals (left-hand side) and corresponding optical power spectra (right-hand side) are typical for the stable-focus regime, which is reached when the optical saturated power is too low to cause reabsorption of the radiation field by the electrons. The low saturated power is caused by the application of a large cavity desynchronization, which drives the optical pulse away quickly from the electron bunch on successive round trips. The fact that (i) the pulse is much longer than in Fig. 5(a) and (ii) the optical power has decreased, reduces the generated second-harmonic signal significantly because of the quadratic dependence on the input power. Therefore, some averaging in the autocorrelation signal was necessary in Fig. 6 to obtain a reasonable signal-to-noise ratio. From the autocorrelation measurements in Figs. 6(a)–6(c) FWHM pulse durations of 4.4, 6.0, and 6.0 ps are derived, respectively. The FWHM spectral widths are, respectively, 0.95%, 0.36%, and 0.55%, leading to time-bandwidth products of 0.50, 0.26, and 0.39, the latter two being close to the expected value of 0.31 for a $\mathrm{sech}^2(t)$-shaped pulse. The longer pulse durations observed in Figs. 6(b) and 6(c) compared to Fig. 6(a) are caused by the fact that at saturation the optical pulse moves away from the electron bunch. When there is still net gain, as in Fig. 6(a), the optical pulse is shorter because of the better overlap with the electron bunch.

V. DISCUSSION

An estimate of the intracavity power will be made in order to compare our results with the model of Hahn and Lee [17]. The intracavity power is related to the power lost by the electrons, ΔP, and the fractional roundtrip loss in the optical cavity, α, as

$$\Delta P = \alpha P_i \ . \tag{8}$$

The parameter α includes the effects of mirror absorption, diffraction, and outcoupling. The energy loss of the

TABLE I. The calculated intracavity (peak) power P_i, synchrotron length L_{syn}, synchrotron frequency Ω, and the nonlinear coupling parameter μ, for three values of the cavity desynchronization ΔL. The FEL wavelength is 24.5 μm at an electron energy of 37.5 MeV.

ΔL (μm)	P_i (GW)	L_{syn} (mm)	Ω (THz)	μ
−3	3	0.7	2.7	1.4
−16	0.7	1.0	1.9	0.94
−50	0.07	1.8	1.1	0.53

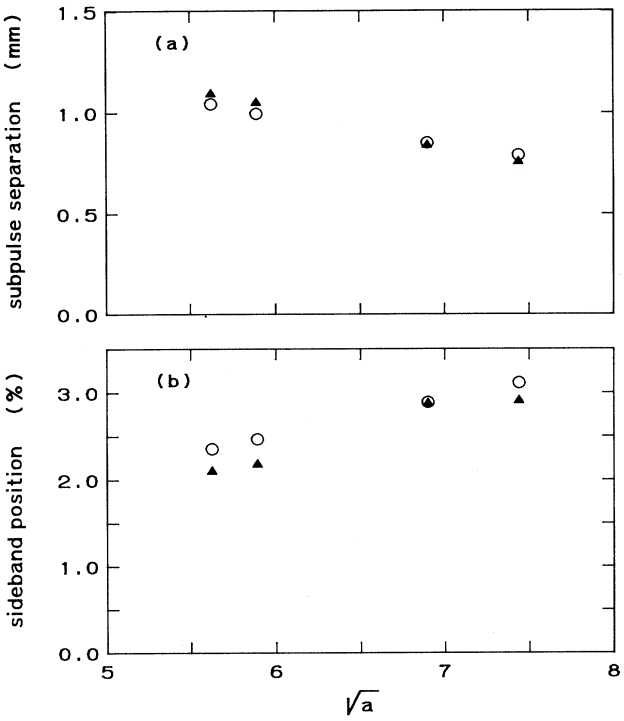

FIG. 7. Position of the subpulse (a) and relative position of the optical sideband (b) versus the square root of the dimensionless optical field a. Solid triangles indicate measurements, open circles indicate calculated values. See Sec. V for details.

electrons was measured with a multichannel spectrometer [30], which is installed behind the undulator. The fractional cavity loss was determined from the exponential decay of the stored field after the electron macropulse is switched off. We found that $\alpha \approx 5\%$ at 24.5 μm wavelength, independent of the cavity detuning [31]. The resulting values of the synchrotron length L_{syn}, the synchrotron oscillation frequency Ω, and the nonlinear coupling parameter μ, as discussed in Sec. III, are given in Table I for the three values of the cavity desynchronism studied in Sec. IV, using the measured FWHM pulse durations at the moment saturation is reached. The FELIX parameters used in the calculation are $\lambda_u = 65$ mm, $K = 1.75$, and $N = 38$.

The values of μ in Table I indicate that FELIX operates in the limit-cycle mode ($0.8 < \mu < 1.5$) for cavity desynchronisms $\Delta L = -3$ μm and -16 μm, i.e., in case (a) and (b) of Fig. 3. The FEL operates in the stable-focus regime ($\mu < 0.8$) for case (c), $\Delta L = -50$ μm. For cases (b) and (c), this is consistent with our experimental observations of the occurrence of macropulse power oscillations and the formation of subpulses. As stated earlier, the discrepancy at $\Delta L = -3$ μm, for which no subpulses are observed, is believed to be due to the fact that the macropulse cannot be sustained long enough for subpulses to develop at the very small desynchronization applied in this case.

According to the model of Hahn and Lee [17], the subpulses are separated by a distance which is equal to the synchrotron length. In the frequency domain, the corresponding sidebands are separated by an amount equal to the synchrotron frequency. We have made a comparison of the model with measurements of the autocorrelation signal and the spectrum, for four cavity desynchronisms in the range -6 μm $< \Delta L < -30$ μm. This includes the case shown in Fig. 3(b). The FEL operates in the limit-cycle mode in all four cases (the parameter μ ranges from 1.18 to 0.89). The measured position of the peak of the first subpulse relative to the initial pulse is shown in Fig. 7(a), as a function of the square root of the dimensionless optical field, $\sqrt{|a|}$. Similarly, the position of the first sideband is shown in Fig. 7(b). These complementary results are both in excellent agreement with the model of Hahn and Lee [17].

In summary, the improved autocorrelator setup has enabled us to make a detailed investigation of the growth and decay of subpulses in the FELIX output. In the range of cavity desynchronism investigated, both the stable-focus mode and the limit-cycle mode have been observed, in perfect agreement with model calculations. Optical pulses as short as 500 fs (FWHM), corresponding to six cycles of the electric field, have been observed with energies of up to 25 μJ (the peak power is 50 MW). The experiments reported here were done at a wavelength of 24.5 μm, but it is worth mentioning that similar observations have been made at other wavelengths in the range from 10 to 32 μm. The results are relevant for other FEL's that (plan to) operate in the regime of strong slippage [8,9].

ACKNOWLEDGMENTS

We are indebted to Professor H. N. Rutt of the University of Southampton for suggesting the use of CdTe as nonlinear crystal. The work described in this paper is part of the research program of the Stichting voor Fundamenteel Onderzoek der Materie (Foundation for Fundamental Research on Matter) and was made possible by the financial support from the Nederlandse Organisatie voor Wetenschappelijk Onderzoek (Netherlands Organization for the Advancement of Research).

[1] A. Dhirani and P. Guyot-Sionnest, Opt. Lett. **20**, 1104 (1995).
[2] F. Seifert, V. Petrov, and M. Woerner, Opt. Lett. **19**, 2009 (1994).
[3] I. M. Bayanov, R. Danielius, P. Heinz, and A. Seilmeier, Opt. Commun. **113**, 99 (1994).
[4] G. Dattoli and A. Renieri, in *Laser Handbook Vol. 4*, edited by M. L. Stitch and M. Bass (North-Holland, Amsterdam, 1985), p. 1.
[5] R. J. Bakker, C. A. J. van der Geer, D. A. Jaroszynski, A. F. G. van der Meer, D. Oepts, and P. W. van Amersfoort, J. Appl. Phys. **74**, 1501 (1993).
[6] D. Oepts, A. F. G. van der Meer, and P. W. van Amersfoort, Infrared Phys. Technol. **36**, 297 (1995).

[7] A. F. G. van der Meer, R. J. Bakker, C. A. J. van de Geer, D. Oepts, P. W. van Amersfoort, W. A. Gillespie, P. F. Martin, and G. Saxon, Nucl. Instrum. Methods Phys. Res. A **331**, 282 (1993).
[8] K. W. Berryman and T. I. Smith, Nucl. Instrum. Methods Phys. Res. A **358**, ABS93 (1995).
[9] R. Prazeres, J. M. Berset, F. Glotin, D. Jaroszynski, and J. M. Ortega, Nucl. Instrum. Methods Phys. Res. A **358**, 212 (1995).
[10] H. Al-Abawi, F. A. Hopf, G. T. Moore, and M. O. Scully, Opt. Commun. **30**, 235 (1979).
[11] R. J. Bakker, D. A. Jaroszynski, A. F. G. van der Meer, D. Oepts, and P. W. van Amersfoort, IEEE J. Quantum Electron. **30**, 1635 (1994).
[12] D. A. Jaroszynski, R. J. Bakker, A. F. G. van der Meer, D. Oepts, and P. W. van Amersfoort, Phys. Rev. Lett. **70**, 3412 (1993).
[13] G. M. H. Knippels, R. F. X. A. M. Mols, A. F. G. van der Meer, D. Oepts, and P. W. van Amersfoort, Phys. Rev. Lett. **75**, 1755 (1995).
[14] R. J. Bakker, G. M. H. Knippels, A. F. G. van der Meer, D. Oepts, D. A. Jaroszynski, and P. W. van Amersfoort, Phys. Rev. E **48**, R3256 (1993).
[15] D. A. Jaroszynski, R. Prazeres, F. Glotin, J. M. Ortega, D. Oepts, A. F. G. van der Meer, G. M. H. Knippels, and P. W. van Amersfoort, Phys. Rev. Lett. **74**, 2224 (1995).
[16] R. W. Warren, J. C. Goldstein, and B. E. Newnam, Nucl. Instrum. Methods Phys. Res. A **250**, 19 (1986).
[17] S. J. Hahn and J. K. Lee, Phys. Rev. E **48**, 2162 (1993).
[18] B. A. Richman, J. M. J. Madey, and E. B. Szarmes, Phys. Rev. Lett. **63**, 1682 (1989).
[19] W. B. Colson, in *Laser Handbook Vol. 6,* edited by W. B. Colson, C. Pellegrini, and A. Renieri (North-Holland, Amsterdam, 1990), pp. 115–194.
[20] N. M. Kroll, P. L. Morton, and M. N. Rosenbluth, IEEE J. Quantum Electron. **17**, 1436 (1981).
[21] S. Riyopoulos, Phys. Plasmas I **9**, 3078 (1994).
[22] A. E. Siegman, *Lasers* (University Science Books, Mill Valley, 1986), p. 666.
[23] M. S. Piltch, C. D. Cantrell, and R. C. Sze, J. Appl. Phys. **47**, 3514 (1976).
[24] E. P. Ippen and C. V. Shank, in *Ultrashort Light Pulses,* edited by S. L. Shapiro (Springer, Berlin, 1977), p. 83.
[25] J. Jansky, G. Corradi, and R. N. Gyuzalian, Opt. Commun. **23**, 293 (1977).
[26] R. Bonifacio, N. Piovella, and B. W. J. McNeil, Phys. Rev. A **44**, R3441 (1991).
[27] K. L. Sala, G. A. Kenny-Wallace, and G. E. Hall, IEEE J. Quantum Electron. **16**, 990 (1980).
[28] R. L. Fork, C. H. Brito Cruz, P. C. Becker, and C. V. Shank, Opt. Lett. **12**, 483 (1987).
[29] A. Stingl, M. Lenzner, Ch. Spielmann, F. Krausz, and R. Szipöcs, Opt. Lett. **20**, 602 (1995).
[30] W. A. Gillespie, A. M. MacLeod, P. F. Martin, G. M. H. Knippels, A. F. G. van der Meer, E. H. Haselhoff, and P. W. van Amersfoort, Nucl. Instrum. Methods Phys. Res. A **358**, 232 (1995).
[31] G. H. C. van Werkhoven, B. Faatz, and G. M. H. Knippels, Opt. Commun. **118**, 551 (1995).

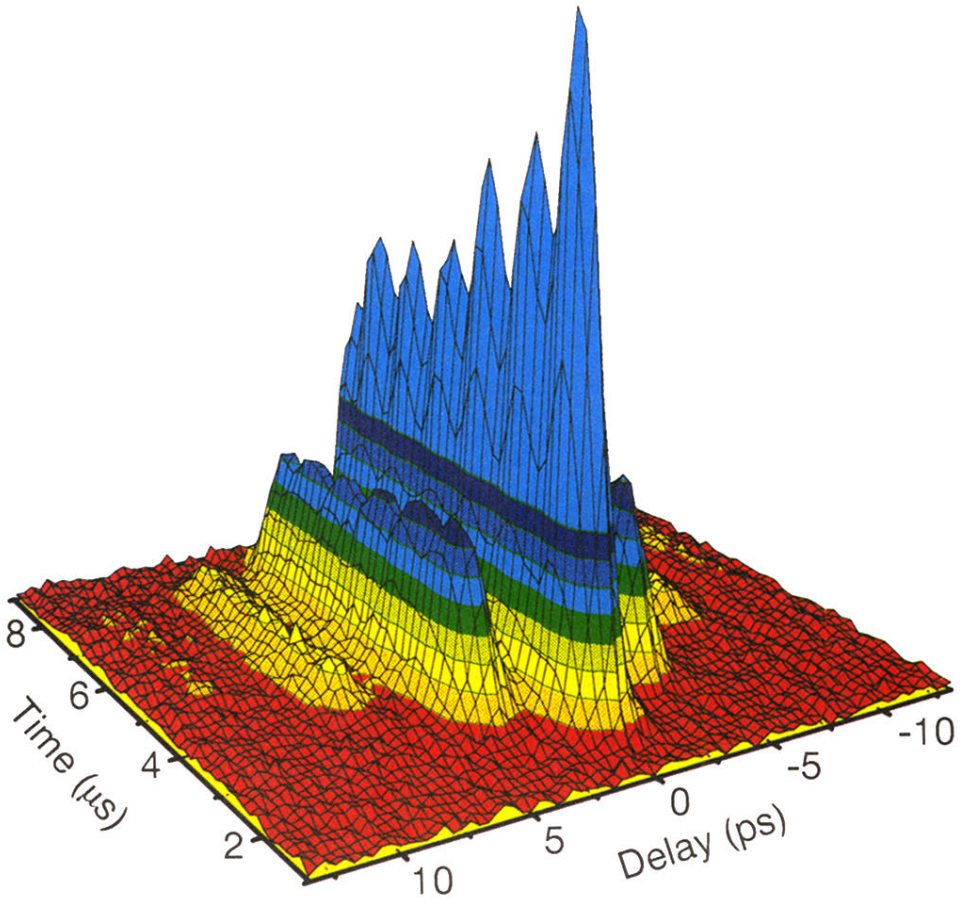

FIG. 2. Second-order autocorrelation signal versus time in the macropulse. The laser wavelength is 24.5 μm and the applied cavity desynchronization ΔL is -16 μm. The development into a train of four separate subpulses is observed (these four pulses show up as seven peaks in the autocorrelation signal). The colors serve for illustration purposes.